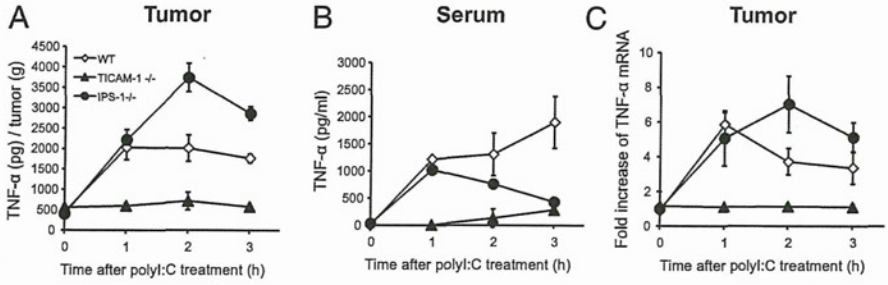

Fig. 2. TNF-α production in tumor and serum of polyI:C-injected 3LL tumor-bearing mice. Mice bearing 3LL tumor were i.p. injected with 200 μg polyI:C. Tumor (*A*) and serum (*B*) were collected at 0, 1, 2, and 3 h after polyI:C injection, and TNF-α concentration was determined by ELISA. TNF-α level in tumor is presented as [TNF-α protein (pg)/tumor weight (g)]. (*C*) Tumors were isolated from polyI:C-injected tumor-bearing WT, TICAM-1$^{-/-}$, and IPS-1$^{-/-}$ mice, and TNF-α mRNA was measured by quantitative PCR; n = 3. Data are shown as average ± SD. A representative experiment of two with similar outcomes is shown.

(Fig. 5*B*). The polyI:C-triggered M1 gene expression continued long in tumor-infiltrated Mfs, a finding that may further explain the tumor-suppressing feature of these Mfs, in addition to the concern of early inducing TNF-α.

Discussion

In this study we demonstrated that the tumor-supporting properties of tumor-infiltrating F4/80$^+$ Mfs characterized by M2 markers are dynamic and able to shift to an M1-dominant state upon the particular signal provided by PRRs. In 3LL tumors that express minimal amounts of MHC class I/II and recruit a large amount of myeloid cells, F4/80$^+$ Mfs function to sustain the tumor in the surrounding microenvironment. This tumor-supporting environment can be disrupted by stimulation with an RNA duplex through a TICAM-1 signal and subsequent induction of mediators such as TNF-α. Thus, the TICAM-1 signal in tumor-infiltrating Mfs plays a key role in TNF-α and M1 shift-mediated tumor regression. These results were confirmed using another cell line, MC38 colon adenocarcinoma (34), although MC38 cells express MHC class I. B16D8 melanoma (12) and EL4 lymphoma (35) were resistant to TNF-α, but their F4/80$^+$ Mfs still possessed TNF-α–inducing potential by stimulation with polyI:C; their susceptibilities to polyI:C reportedly depend on other effectors (12, 35). These results may partly explain the reported findings that tumors regressed in patients with simultaneous virus infection (36, 37), and that tumor growth was inhibited by polyI:C injection in tumor-bearing mice (6, 7).

In contrast, polyI:C-stimulated PEC or bone marrow-derived Mfs induce type I IFN via the IPS-1 pathway unlike the case of tumor-infiltrating F4/80$^+$ Mfs. Nevertheless, all of these Mf subsets produce proinflammatory cytokines, including TNF-α, in a TICAM-1–dependent manner. Thus, the key question that arose was why predominant TICAM-1 dependence for polyI:C-mediated production of TNF-α occurred in F4/80$^+$ tumor-infiltrating Mfs leading to tumor regression. A marked finding is that the TLR3 protein level is high in tumor-infiltrating Mfs compared with other sources of Mfs (Fig. S10). In addition, the IPS-1 pathway is unresponsive to polyI:C if the polyI:C is exogenously added to the tumor-infiltrating Mfs without transfection reagents. The cytoplasmic dsRNA sensors normally work for IFN induction in tumor F4/80$^+$ Mfs if the polyI:C is transfected into the cells. TICAM-1–dependent TNF-α production by F4/80$^+$ Mfs (Fig. S11 *D* and *F*) occurs partly because F4/80$^+$ Mfs express a high basal level of TLR3 and fail to take up extrinsic polyI:C into the cytoplasm. Of many subsets of Mfs, these properties (38) are unique to the F4/80$^+$ Mfs.

Hemorrhagic necrosis and tumor size reduction are closely correlated with constitutive production of TNF-α (39, 40). The association of PRR-derived TNF-α and hemorrhagic necrosis of tumor has been described earlier. Carswell et al. (41) showed that TNF-α is robustly expressed in mouse serum following treatment with bacillus Calmette–Guérin and endotoxin. Bioassay of TNF-α as reflected by the degree of hemorrhagic necrosis of transplanted Meth A sarcoma in BALB/c mice led the authors to speculate that Mfs are responsible for TNF-α induction. Many years later, Dougherty et al. (42) identified the mechanism responsible for the TNF-α production associated with antitumor activity; macrophages isolated from tumors in mice with inactivating mutation in the TLR4 gene [Lps(d) in C3H/HeJ] expressed 5- to 10-fold less TNF-α than tumors in WT mice. This finding represents a unique recognition of a PRR contributing to the cancer phenotype. Subsequent studies determined that MyD88 is involved in the induction of TNF-α via TLR4 binding to its cognate ligand, lipid A endotoxin (15, 43). Because the TLR3 signal is independent of MyD88, this MyD88 concept is not applicable to the present study on polyI:C-dependent tumor regression.

Alternatively, endotoxin/lipid A may have activated TICAM-1 in previous reports on TLR4-derived TNF-α because TLR4 can recruit TICAM-1 in addition to MyD88 (15). The lipid A derivative monophospholipid A preferentially activates the TICAM-1 pathway of TLR4 (43). It is likely that TICAM-1 participates in TLR4-mediated tumor regression in addition to MyD88, although MyD88 is not involved in the polyI:C signaling. This point was further proven using TNF-α$^{-/-}$ mice: TICAM-1–derived TNF-α in F4/80$^+$ Mf cells has a critical role in the induction of tumor necrosis and regression by polyI:C. The results are consistent with the finding that both TICAM-1 and IPS-1 pathways are able to induce NF-κB activation secondary to polyI:C stimulation, and indeed their signals converge at the IκB kinase complex (18).

TICAM-1 is able to induce many of the IFN-inducible genes that MyD88 cannot in mDCs (44). In both cases of TICAM-1 and MyD88 stimulation, tumor-infiltrating Mfs facilitate the expression of many genes in addition to TNF-α. The M2 phenotype of F4/80$^+$ Mfs or tumor-associated Mfs is modified dependent on these additional factors. IFNAR facilitates polyI:C-mediated tumor regression in tumor-bearing mice, lack of which results in no induction of TLR3 (Fig. S7). Thus, preceding the polyI:C

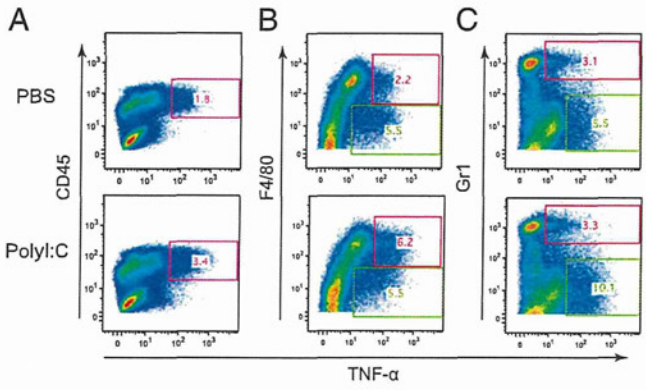

Fig. 3. F4/80$^+$ cells are responsible for the polyI:C-induced elevation of TNF-α production in tumor. Mice bearing 3LL tumors were i.p. injected with 200 μg polyI:C. TNF-α–producing cells in tumors of polyI:C- or PBS-injected mice were examined by immunohistochemical staining and flow cytometry to determine intracellular cytokine expression profiles of CD45$^+$ cells (*A*), F4/80$^+$ cells (*B*), and Gr1$^+$ cells (*C*). CD45$^+$ cells in tumor were gated and are shown in *B* and *C*. A representative experiment of two with similar outcomes is shown. TNF-α$^+$ gating squares are shown in red (positive) and green (negative).

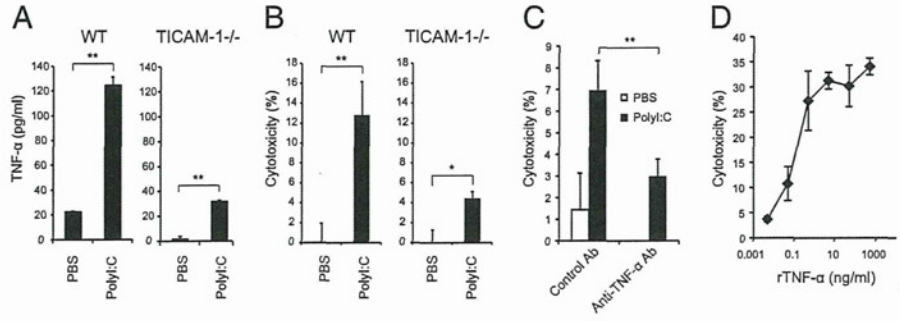

Fig. 4. PolyI:C enhances TNF-α production and cytotoxicity of F4/80$^+$ cells in tumor. PolyI:C (200 μg) or PBS was i.p. injected into 3LL tumor-bearing WT mice. After 30 min, F4/80$^+$ cells isolated from tumor were cultured for 24 h and TNF-α concentration in the conditioned medium was determined by ELISA (*A*). In parallel, the cytotoxicity of tumor-infiltrating F4/80$^+$ cells against 3LL tumor cells was measured by ^{51}Cr-release assay (*B*). Anti–TNF-α neutralization antibody or control antibody was added (10 μg/mL) to mixed culture of isolated tumor-infiltrating F4/80$^+$ cells and 3LL tumor cells (*C*). (*D*) Cytotoxic activity of TNF-α against 3LL tumor cells. Recombinant TNF-α was added to ^{51}Cr-labeled 3LL tumor cell culture at various concentrations. After 20 h, cytotoxicity was measured; $n = 3$. Data are shown as average ± SD. $*P < 0.05$, $**P < 0.001$. A representative experiment of three with similar outcomes is shown.

response, minute type I IFN of undefined source has to be provided to set the TLR3/TICAM-1 pathway, which may primarily fail in IFNAR$^{-/-}$ mice. Cellular effectors, cytotoxic T lymphocyte (CTL) and NK cells, are induced secondary to activation of IFN-inducible genes in a late phase of polyI:C-stimulated myeloid cells (45–47). The relationship among the TICAM-1–mediated type I IFN liberation, these late-phase effectors, and tumor regression remains an open question in this setting.

M1 Mf cells function to protect the host against tumors by producing large amounts of inflammatory cytokines and activating the immune response (48, 49). However, distinct types of M2 cells differentiate when monocytes are stimulated with IL-4 and IL-13 (M2a), immune complexes/TLR ligands (M2b), or IL-10 and glucocorticoids (M2c) (50). In our study, polyI:C stimulation led to incremental expression of the M1 Mf-related genes. In contrast, polyI:C stimulation was not associated with M2 polarization, except for IL-10. Other genes related to angiogenesis and extravasation were not affected by polyI:C treatment. Thus, polyI:C was able to induce the characteristic M1 conversion and, in turn, contribute to tumor regression. It is notable that TAM cells usually have defective and delayed NF-κB activation in response to different proinflammatory signals, such as expression of cytotoxic mediators NO, cytokines, TNF-α, and IL-12 (51–53). These observations are in apparent contrast with the function of other resident Mf species. This discrepancy may again reflect a dynamic change in the tumor microenvironment during tumor progression.

In line with our findings, virus infection has been observed to instigate tumor regression in patients with cancer (36, 54). Gene therapy for cancer patients using virus-derived vectors has proved effective in reducing tumors in clinic (36, 37). Administration of dsRNA elicits IFN induction, NK cell activation, and CTL proliferation for antitumor effectors in vivo (19, 55). This is a unique finding that tumor-infiltrating Mfs are a target of dsRNA and converted from tumor supporters to tumoricidal effectors. Hence, the antitumor effect of dsRNA adjuvant is ultimately based on the liberation of type I IFN, functional maturation of mDCs, and modulation of tumor-infiltrating Mfs, where TICAM-1 is a crucial transducer in eliciting antitumor immunity.

Methods

Inbred C57BL/6 WT mice were purchased from CLEA Japan, Inc. TICAM-1$^{-/-}$ and IPS-1$^{-/-}$ mice were generated in our laboratory and maintained as described previously. IRF-3/7 double-KO mice were a gift from T. Taniguchi

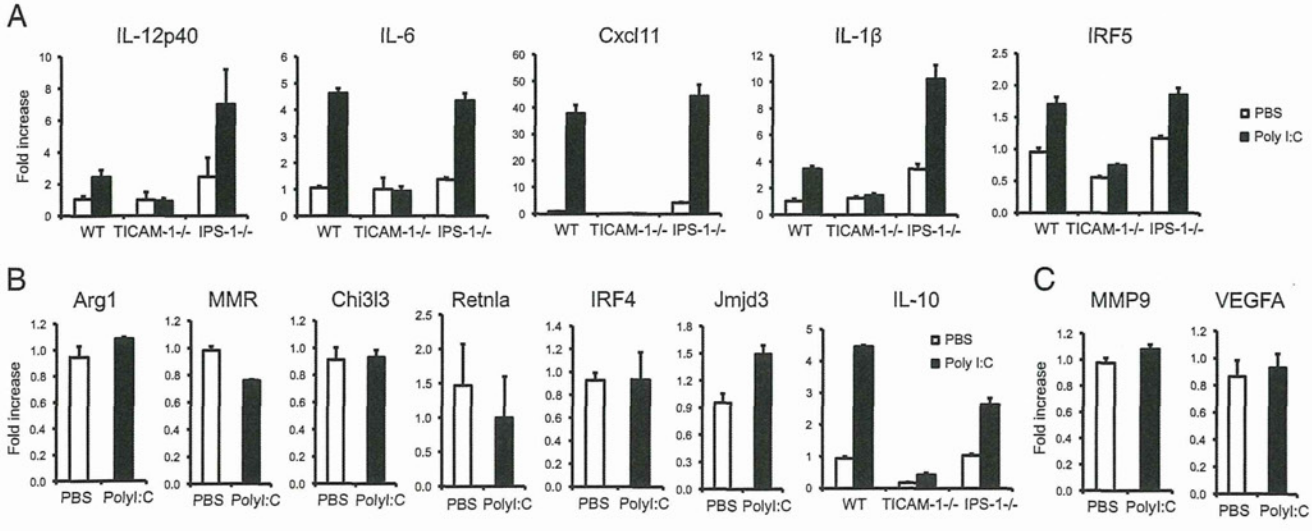

Fig. 5. PolyI:C induces M1 polarization of TAMs. F4/80$^+$ cells were isolated from 3LL tumor and stimulated with polyI:C (50 μg/mL) for 4 h. Total RNA was extracted and used to analyze the transcript expression levels of M1 (*A*) and M2 (*B* and *C*) markers; $n = 3$. Data are shown as average ± SD. A representative experiment of two with similar outcomes is shown.

(University of Tokyo, Tokyo, Japan). TNF-$\alpha^{-/-}$ mice were kindly provided by A. Nakane (Hirosaki University, Aomori, Japan) and Y. Iwakura (University of Tokyo). Mice 6–10 wk of age were used in all experiments. 3LL lung cancer cells were cultured at 37 °C under 5% CO_2 in RPMI containing 10% FCS, penicillin, and streptomycin. This study was carried out in strict accordance with the recommendations in the Guide for the Care and Use of Laboratory Animals of the National Institutes of Health. The protocol was approved by the Committee on the Ethics of Animal Experiments in the Animal Safety Center, Hokkaido University, Japan. All mice were used according to the guidelines of the Institutional Animal Care and Use Committee of Hokkaido University, who approved this study as no. 08-0290, "Analysis of Anti-Tumor Immune Response Induced by the Activation of Innate Immunity."

Other detailed methods are provided in *SI Methods*.

ACKNOWLEDGMENTS. We thank Dr. T. Taniguchi (University of Tokyo) and D. M. Segal (EIB/NCI, Bethesda, MD) for kindly providing us with IRF-3/7 double KO mice and mAb against mouse TLR3. This work was supported in part by Grants-in-Aid from the Ministry of Education, Science, and Culture (MEXT), "the Carcinogenic Spiral" a MEXT Grant-in-Project, and the Ministry of Health, Labor, and Welfare of Japan, the Takeda Foundation, the Akiyama Foundation, and the Waxman Foundation.

1. Grivennikov SI, Greten FR, Karin M (2010) Immunity, inflammation, and cancer. *Cell* 140:883–899.
2. de Visser KE, Eichten A, Coussens LM (2006) Paradoxical roles of the immune system during cancer development. *Nat Rev Cancer* 6:24–37.
3. Chan AT, Ogino S, Fuchs CS (2007) Aspirin and the risk of colorectal cancer in relation to the expression of COX-2. *N Engl J Med* 356:2131–2142.
4. Rakoff-Nahoum S, Medzhitov R (2007) Regulation of spontaneous intestinal tumorigenesis through the adaptor protein MyD88. *Science* 317:124–127.
5. Chen GY, Shaw MH, Redondo G, Núñez G (2008) The innate immune receptor Nod1 protects the intestine from inflammation-induced tumorigenesis. *Cancer Res* 68: 10060–10067.
6. Sarma PS, Shiu G, Neubauer RH, Baron S, Huebner RJ (1969) Virus-induced sarcoma of mice: Inhibition by a synthetic polyribonucleotide complex. *Proc Natl Acad Sci USA* 62: 1046–1051.
7. Levy HB, Law LW, Rabson AS (1969) Inhibition of tumor growth by polyinosinic-polycytidylic acid. *Proc Natl Acad Sci USA* 62:357–361.
8. Absher M, Stinebring WR (1969) Toxic properties of a synthetic double-stranded RNA. Endotoxin-like properties of poly I. poly C, an interferon stimulator. *Nature* 223: 715–717.
9. Talmadge JE, et al. (1985) Immunomodulatory effects in mice of polyinosinic-polycytidylic acid complexed with poly-L-lysine and carboxymethylcellulose. *Cancer Res* 45: 1058–1065.
10. Longhi MP, et al. (2009) Dendritic cells require a systemic type I interferon response to mature and induce $CD4^+$ Th1 immunity with poly IC as adjuvant. *J Exp Med* 206: 1589–1602.
11. Matsumoto M, Seya T (2008) TLR3: Interferon induction by double-stranded RNA including poly(I:C). *Adv Drug Deliv Rev* 60:805–812.
12. Akazawa T, et al. (2007) Antitumor NK activation induced by the Toll-like receptor 3-TICAM-1 (TRIF) pathway in myeloid dendritic cells. *Proc Natl Acad Sci USA* 104: 252–257.
13. Miyake T, et al. (2009) Poly I:C-induced activation of NK cells by CD8 alpha+ dendritic cells via the IPS-1 and TRIF-dependent pathways. *J Immunol* 183:2522–2528.
14. McCartney S, et al. (2009) Distinct and complementary functions of MDA5 and TLR3 in poly(I:C)-mediated activation of mouse NK cells. *J Exp Med* 206:2967–2976.
15. Oshiumi H, Matsumoto M, Funami K, Akazawa T, Seya T (2003) TICAM-1, an adaptor molecule that participates in Toll-like receptor 3-mediated interferon-beta induction. *Nat Immunol* 4:161–167.
16. Yoneyama M, et al. (2005) Shared and unique functions of the DExD/H-box helicases RIG-I, MDA5, and LGP2 in antiviral innate immunity. *J Immunol* 175:2851–2858.
17. Takeuchi O, Akira S (2010) Pattern recognition receptors and inflammation. *Cell* 140: 805–820.
18. Sasai M, et al. (2006) NAK-associated protein 1 participates in both the TLR3 and the cytoplasmic pathways in type I IFN induction. *J Immunol* 177:8676–8683.
19. Seya T, Matsumoto M (2009) The extrinsic RNA-sensing pathway for adjuvant immunotherapy of cancer. *Cancer Immunol Immunother* 58:1175–1184.
20. Iwasaki A, Medzhitov R (2010) Regulation of adaptive immunity by the innate immune system. *Science* 327:291–295.
21. Condeelis J, Pollard JW (2006) Macrophages: Obligate partners for tumor cell migration, invasion, and metastasis. *Cell* 124:263–266.
22. Schuler G, Schuler-Thurner B, Steinman RM (2003) The use of dendritic cells in cancer immunotherapy. *Curr Opin Immunol* 15:138–147.
23. Murdoch C, Muthana M, Coffelt SB, Lewis CE (2008) The role of myeloid cells in the promotion of tumour angiogenesis. *Nat Rev Cancer* 8:618–631.
24. Borrello MG, Degl'Innocenti D, Pierotti MA (2008) Inflammation and cancer: The oncogene-driven connection. *Cancer Lett* 267:262–270.
25. Biswas SK, Mantovani A (2010) Macrophage plasticity and interaction with lymphocyte subsets: Cancer as a paradigm. *Nat Immunol* 11:889–896.
26. Farma JM, et al. (2007) Direct evidence for rapid and selective induction of tumor neovascular permeability by tumor necrosis factor and a novel derivative, colloidal gold bound tumor necrosis factor. *Int J Cancer* 120:2474–2480.
27. Masuda H, et al. (2002) High levels of RAE-1 isoforms on mouse tumor cell lines assessed by the anti-pan-Rae-1 polyclonal antibody confers tumor cell cytotoxicity on mouse NK cells. *Biochem Biophys Res Commun* 290:140–145.
28. Smyth MJ, et al. (2004) NKG2D recognition and perforin effector function mediate effective cytokine immunotherapy of cancer. *J Exp Med* 200:1325–1335.
29. Remels L, Fransen L, Huygen K, De Baetselier P (1990) Poly I:C activated macrophages are tumoricidal for TNF-α-resistant 3LL tumor cells. *J Immunol* 144:4477–4486.
30. Jelinek I, et al. (2011) TLR3-specific double-stranded RNA oligonucleotide adjuvants induce dendritic cell cross-presentation, CTL responses, and antiviral protection. *J Immunol* 186:2422–2429.
31. Krausgruber T, et al. (2011) IRF5 promotes inflammatory macrophage polarization and TH1-TH17 responses. *Nat Immunol* 12:231–238.
32. Satoh T, et al. (2010) The Jmjd3-*Irf4* axis regulates M2 macrophage polarization and host responses against helminth infection. *Nat Immunol* 11:936–944.
33. De Santa F, et al. (2007) The histone H3 lysine-27 demethylase Jmjd3 links inflammation to inhibition of polycomb-mediated gene silencing. *Cell* 130:1083–1094.
34. Zitvogel L, et al. (1995) Cancer immunotherapy of established tumors with IL-12. Effective delivery by genetically engineered fibroblasts. *J Immunol* 155:1393–1403.
35. Abe R, Peng T, Sailors J, Bucala R, Metz CN (2001) Regulation of the CTL response by macrophage migration inhibitory factor. *J Immunol* 166:747–753.
36. Russell SJ (2002) RNA viruses as virotherapy agents. *Cancer Gene Ther* 9:961–966.
37. Aghi M, Martuza RL (2005) Oncolytic viral therapies—the clinical experience. *Oncogene* 24:7802–7816.
38. Watanabe A, et al. (2011) Raftlin is involved in the nucleocapture complex to induce poly(I:C)-mediated TLR3 activation. *J Biol Chem* 286:10702–10711.
39. Mocellin S, Rossi CR, Pilati P, Nitti D (2005) Tumor necrosis factor, cancer and anticancer therapy. *Cytokine Growth Factor Rev* 16:35–53.
40. Balkwill F (2009) Tumour necrosis factor and cancer. *Nat Rev Cancer* 9:361–371.
41. Carswell EA, et al. (1975) An endotoxin-induced serum factor that causes necrosis of tumors. *Proc Natl Acad Sci USA* 72:3666–3670.
42. Dougherty ST, Eaves CJ, McBride WH, Dougherty GJ (1997) Molecular mechanisms regulating TNF-alpha production by tumor-associated macrophages. *Cancer Lett* 111: 27–37.
43. Mata-Haro V, et al. (2007) The vaccine adjuvant monophosphoryl lipid A as a TRIF-biased agonist of TLR4. *Science* 316:1628–1632.
44. Ebihara T, et al. (2010) Identification of a polyI:C-inducible membrane protein that participates in dendritic cell-mediated natural killer cell activation. *J Exp Med* 207: 2675–2687.
45. Akazawa T, et al. (2004) Adjuvant-mediated tumor regression and tumor-specific cytotoxic response are impaired in MyD88-deficient mice. *Cancer Res* 64:757–764.
46. Akazawa T, et al. (2007) Tumor immunotherapy using bone marrow-derived dendritic cells overexpressing Toll-like receptor adaptors. *FEBS Lett* 581:3334–3340.
47. Schulz O, et al. (2005) Toll-like receptor 3 promotes cross-priming to virus-infected cells. *Nature* 433:887–892.
48. Mantovani A, Sica A, Locati M (2007) New vistas on macrophage differentiation and activation. *Eur J Immunol* 37:14–16.
49. Martinez FO, Helming L, Gordon S (2009) Alternative activation of macrophages: An immunologic functional perspective. *Annu Rev Immunol* 27:451–483.
50. Mantovani A, et al. (2004) The chemokine system in diverse forms of macrophage activation and polarization. *Trends Immunol* 25:677–686.
51. Sica A, et al. (2000) Autocrine production of IL-10 mediates defective IL-12 production and NF-kappa B activation in tumor-associated macrophages. *J Immunol* 164:762–767.
52. Torroella-Kouri M, et al. (2005) Diminished expression of transcription factors nuclear factor kappaB and CCAAT/enhancer binding protein underlies a novel tumor evasion mechanism affecting macrophages of mammary tumor-bearing mice. *Cancer Res* 65: 10578–10584.
53. Biswas SK, et al. (2006) A distinct and unique transcriptional program expressed by tumor-associated macrophages (defective NF-kappaB and enhanced IRF-3/STAT1 activation). *Blood* 107:2112–2122.
54. Bluming AZ, Ziegler JL (1971) Regression of Burkitt's lymphoma in association with measles infection. *Lancet* 2:105–106.
55. Matsumoto M, Oshiumi H, Seya T (2011) Antiviral responses induced by the TLR3 pathway. *Rev Med Virol* 21:67–77.

Supporting Information

Shime et al. 10.1073/pnas.1113099109

SI Methods

Reagents. PolyI:C was purchased from GE Healthcare, which was free from LPS contamination. TNF-α and IFN-β ELISA kit was purchased from eBioscience and PBL InterferonSource, respectively. Recombinant TNF-α was purchased from R&D Systems.

Tumor Cells and Tumor-Infiltrated Immune Cells. We first tested the amounts of macrophages (Mfs) in implant tumors formed in B6 mice. Mouse lymphoma (EL4), Lewis lung carcinoma (3LL), adenocarcinoma MC38, and melanoma (B16D8) lines grew well in the back of mice, and the Mf content was maximal in the 3LL tumor. MC38, a murine colon adenocarcinoma cell line, was a gift from S. A. Rosenberg (National Cancer Institute, Bethesda) (1). Hemorrhagic necrosis shown in Fig. 1*A* was typically induced in response to polyI:C in 3LL tumor. We then used the 3LL line for this study.

3LL cells were found to express very low amounts of detectable MHC class I or class II (Table S1), suggesting this cell type as a possible target for natural killer (NK) cells but not cytotoxic T lymphocytes (CTLs). 3LL cells were found to express appreciable amounts of the NKG2D ligand, retinoic acid-inducible gene 1, consistent with previous reports (Table S1) (2, 3). 3LL cells also expressed mRNA transcripts for Toll-like receptor 3 (TLR3), Toll–IL-1 receptor domain-containing adaptor molecule 1 (TICAM-1), IFN-β promoter stimulator 1 (IPS-1), and melanoma differentiation-associated protein 5 (MDA5). Exposure to polyI:C-stimulated peritoneal Mfs caused significant death of 3LL cells, which was likely an effect of liberated inflammatory cytokines such as TNF-α (4). Consistent with previously reported data about 3LL properties in vitro, the 3LL cells we used were not damaged by direct polyI:C treatment or exposure to 3LL-derived cytokines (Fig. S8*C*). When 3LL cells were implanted s.c. in mice, the resulting tumors were found to contain a high amount (>30%) of $CD45.2^+$ cells (Fig. S5*A*). The major population of those $CD45.2^+$ cells was determined to be of $CD11b^+$ myeloid lineage cells that coexpressed $F4/80^+$, $Gr1^+$, or $CD11c^+$. A small population of $NK1.1^+$ cells was also detected. $CD4^+$ T cells, $CD8^+$ T cells, and B cells were rarely detected in these implant tumors (Fig. S5*A*).

Cytotoxic Activity Assay. Mice bearing 3LL tumor were injected i.p. with polyI:C. Mice were killed and $F4/80^+$ cells were isolated from tumor by using MACS-positive selection beads (Miltenyi) as described previously. 3LL cells were labeled with ^{51}Cr for 3–5 h and then washed three times with the medium. $F4/80^+$ cells, and 3LL cells were cocultured at the indicated ratio. After 20 h, supernatants were harvested and ^{51}Cr release was measured in each sample. Specific lysis was calculated by the following formula: cytotoxicity (%) = [(experimental release − spontaneous release)/(max release − spontaneous release)] × 100.

Flow Cytometric Analysis. Mononuclear cells prepared from spleen and tumor were treated with anti-CD16/32 (no. 93) and stained with APC–anti-CD45.2 (no. 104), FITC–anti-CD11b (M1/70), PE–anti-GR1 (RB6-8C5), FITC–anti-CD11c (N418), PE– or APC–anti-F4/80 (BM8), PE–anti-NK1.1 (PK136), PE–anti-CD49b (DX5), PE–anti-CD3e (145-2C11), FITC–anti-CD4 (GK1.5), FITC–anti-CD8a (53-6.7), and PE- and anti-CD19 (MB19-1; eBioscience and Biolegend; Table S2). Samples were analyzed with FACSCalibur (BD Biosciences), and data analysis was performed using FlowJo software (Tree Star). For intracellular cytokine staining, we freshly isolated tumors from polyI:C or PBS-injected mice at 1 h and incubated the cells in the presence of 10 μg/mL Brefeldin A for 3 h. Cells were fixed and stained with the combination of anti-CD45.2 Ab and anti-F4/80 Ab or anti-Gr1 Ab, followed by permeabilizing and staining with anti-TNF Ab using BD Cytofix/Cytoperm Kit (BD Biosciences).

Quantitative PCR Analysis. Tumor samples were cut into small pieces and homogenized with TRIzol Reagent (Invitrogen). Total RNA was isolated according to the manufacturer's instruction. Reverse transcription was performed using High-Capacity cDNA Reverse Transcription Kit (Applied Biosystems). Real-time PCR was performed with Power SYBR Green PCR Master Mix (Applied Biosystems) with a StepOne Real-Time PCR System (Applied Biosystems). Expression of the cytokine gene was normalized to the expression of *GAPDH*. We used primer pairs listed in Table S3. Data were analyzed by the ΔΔCt method.

ELISA and Cytokine Beads Assay. Tumor samples were cut into small pieces and homogenized with CelLytic MT Mammalian Tissue Lysis/Extraction Reagent (Sigma) supplemented with Complete Protease Inhibitor Mixture (Roche) on ice. Lysate was centrifuged to remove insoluble materials, and the supernatant was used for ELISA. Serum cytokine concentration was determined by ELISA or cytokine bead assays. Data were shown as TNF-α (pg) per weight of tumor (g).

Histochemistry and Immunohistochemistry. 3LL tumor was fixed with buffered 10% formalin overnight and embedded in paraffin wax, and sections 4 μm in thickness were stained with H&E. For immunohistochemistry, tumor was embedded in optimal cutting-temperature compound, and snap-frozen in liquid nitrogen. Cryosections 6 μm in thickness were air-dried for 60 min and fixed for 15 min with prechilled acetone and then incubated with FITC–anti-CD31 antibody (390; BioLegend). The sections were mounted in Prolong Gold Antifade Reagent with DAPI (Invitrogen). Images were obtained with a Leica LSM510 confocal laser-scanning microscope.

Tumor Challenge and PolyI:C Treatment. Mice were shaved at the back and injected s.c with 200 μL of 3×10^6 3LL cells in PBS(−). Tumor size was measured using a caliper. Tumor volume was calculated using the following formula: tumor volume (cm^3) = (long diameter) × (short diameter)^2 × 0.4. PolyI:C (250 μg/head) with no detectable LPS was injected i.p. as indicated. In some cases, polymixin B-treated polyI:C was used. When an average tumor volume of 0.5–0.8 cm^3 was reached, the treatment was started and repeated every 4 d.

Isolation of $F4/80^+$ Cells from Tumor. Tumors formed by 3LL cells were excised at 2 wk after transplantation and treated with 0.05 mg/mL Collagenase I (Sigma), 0.05 mg/mL Collagenase IV (Sigma), 0.025 mg/mL hyaluronidase (Sigma), and 0.01 mg/mL DNase I (Roche) in HBSS at 37 °C for 10 min. $F4/80^+$ cells were isolated by using biotinylated anti-F4/80 antibody (BM8) and Streptavidin MicroBeads (Miltenyi). We routinely prepared $F4/80^+$ cells at >90% purity from tumor.

1. Zitvogel L, et al. (1995) Cancer immunotherapy of established tumors with IL-12. Effective delivery by genetically engineered fibroblasts. *J Immunol* 155:1393–1403.
2. Masuda H, et al. (2002) High levels of RAE-1 isoforms on mouse tumor cell lines assessed by the anti-pan-Rae-1 polyclonal antibody confers tumor cell cytotoxicity on mouse NK cells. *Biochem Biophys Res Commun* 290:140–145.
3. Smyth MJ, et al. (2004) NKG2D recognition and perforin effector function mediate effective cytokine immunotherapy of cancer. *J Exp Med* 200:1325–1335.
4. Remels L, Fransen L, Huygen K, De Baetselier P (1990) Poly I:C activated macrophages are tumoricidal for TNF-α-resistant 3LL tumor cells. *J Immunol* 144:4477–4486.

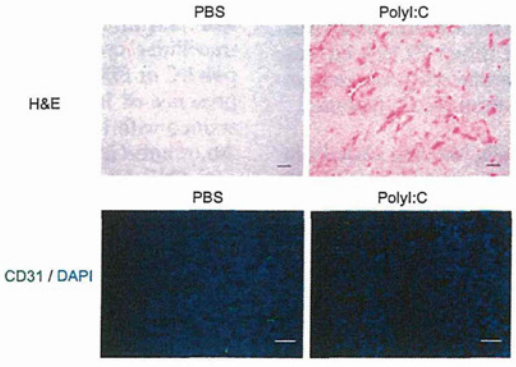

Fig. S1. Poly I:C induces hemorrhagic necrosis of tumor. 3LL tumor-bearing mice were i.p. injected with 200 μg poly I:C and tumors were isolated 12 h later. Formalin-fixed tumors stained with H&E (*Upper*) and frozen sections stained with anti-CD31 antibody and DAPI nuclear stain (*Lower*). Original magnification 10× for all panels. (Scale bars, 100 μm.) A representative experiment of three with similar outcomes is shown.

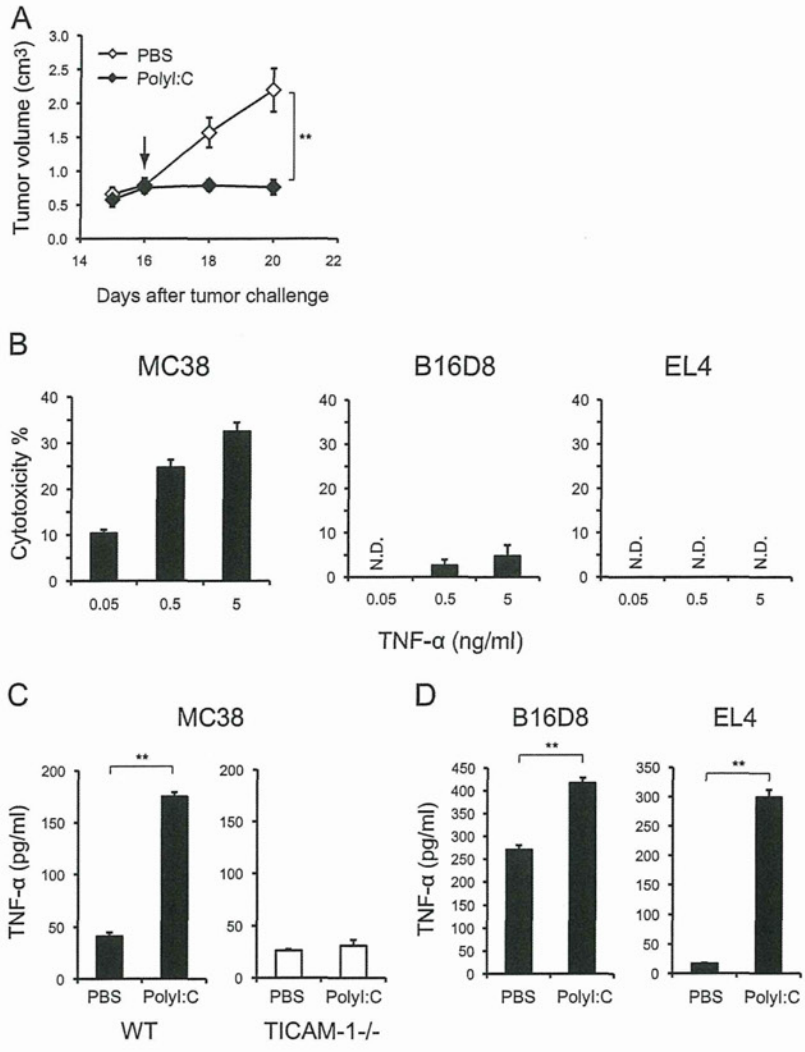

Fig. S2. Poly:C induces TNF-α production by tumor-associated F4/80$^+$ Mfs in various types of tumor. (*A*) MC38 cells (1×10^5) were s.c implanted into C57BL/6 mice (day 0). Poly:C (200 μg) was i.p. injected on day 16. Data are shown as tumor average size ± SE; $n = 3$–4 mice per group. (*B*) Sensitivity of MC38, B16D8, and EL4 cells to recombinant TNF-α. (*C* and *D*) MC38, B16D8, and EL4 tumor-bearing mice were i.p injected with 200 μg poly:C. After 1 h, F4/80$^+$ cells were isolated from tumors and incubated for 24 h. TNF-α concentration in the conditioned medium was determined by ELISA; $n = 3$. Data are shown as average ± SD. N.D., not detected. A representative experiment of two with similar outcomes is shown.

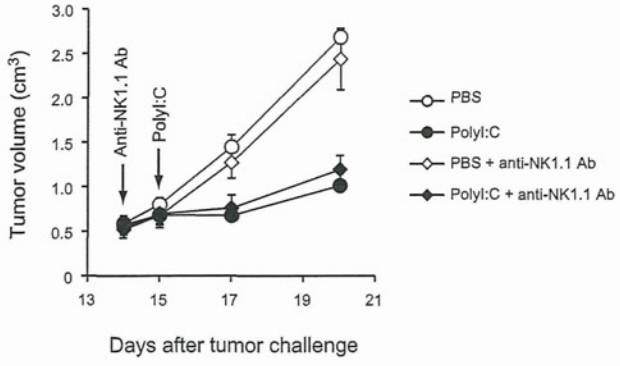

Fig. S3. NK cells are not essential for poly:C-induced antitumor activity in vivo. 3LL tumor cells (3×10^6) were s.c transplanted into C57BL/6 mice (day 0). NK cells were depleted by injection of anti-NK1.1 antibody (PK136) into 3LL tumor-bearing mice on day 14. All doses of antibody and treatment regimens were determined in preliminary studies using the same lot of antibodies used for the experiments. Treatment was confirmed to deplete completely the desired cell populations for the entire duration of the study. Poly:C (250 μg) was i.p injected on day 15 and the tumor volume was measured. Data shown are means ± SE, $n = 3$. A representative experiment of two with similar outcomes is shown.

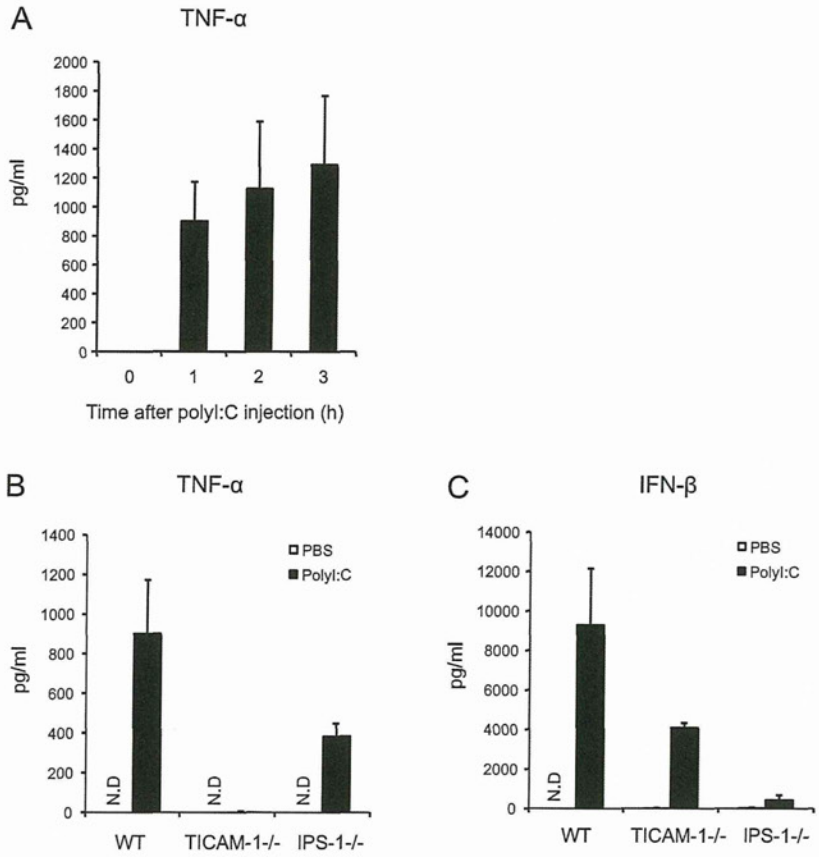

Fig. S4. Cytokine production in polyI:C-treated mouse. (*A*) WT mice were injected i.p with 200 μg polyI:C. After 0, 1, 2, and 3 h, TNF-α concentration in serum was determined by ELISA. (*B* and *C*) WT, TICAM-1$^{-/-}$, and IPS-1$^{-/-}$ mice were injected i.p with 200 μg polyI:C. After 1 h for TNF-α (*B*) and 4 h for IFN-β (*C*), serum cytokine levels were determined by ELISA. Data represents mean ± SD (n = 3). N.D., not detected. A representative experiment of three with similar outcomes is shown.

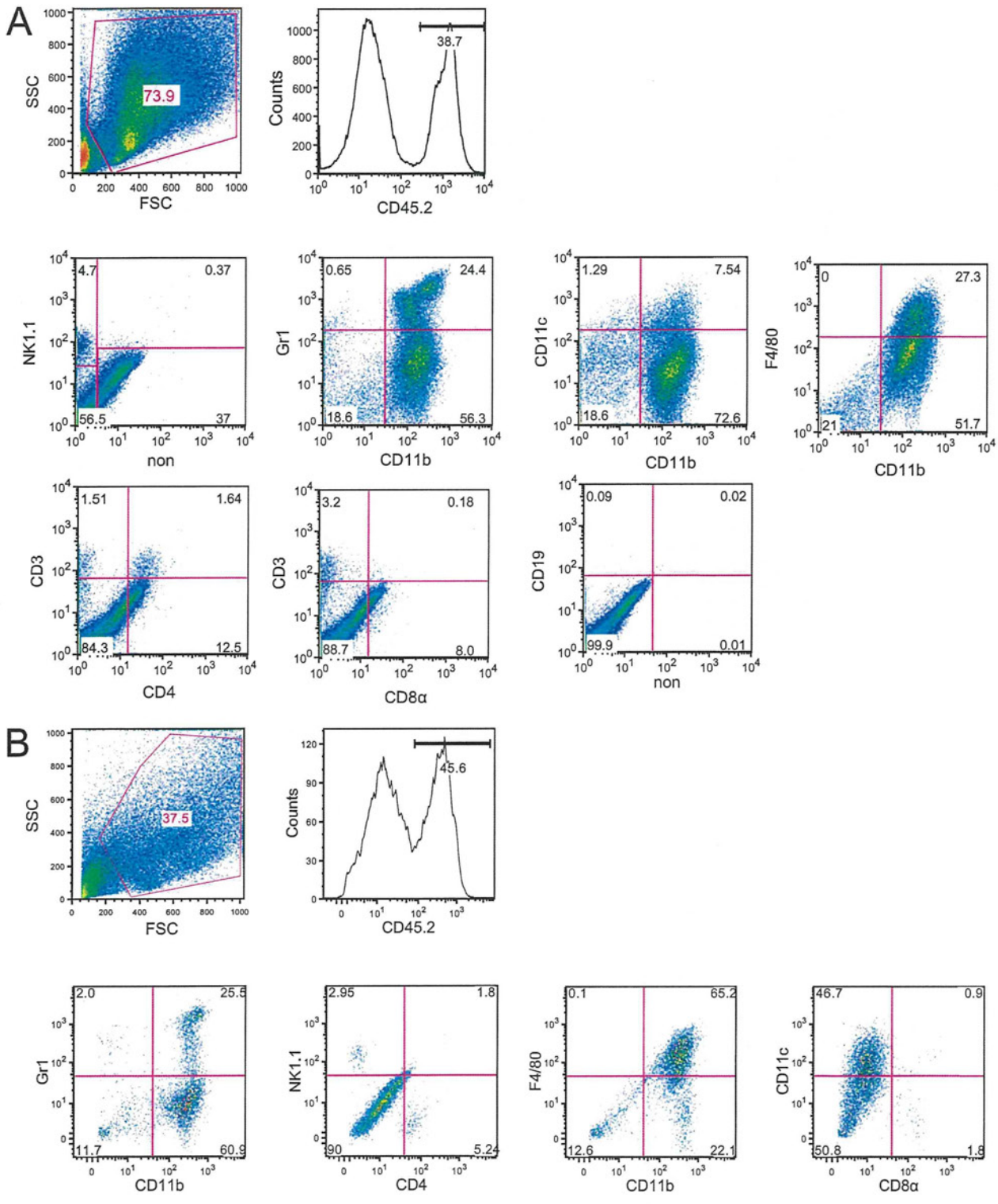

Fig. S5. Analysis of immune cells infiltrated into tumor. 3LL tumor cells (3×10^6) (*A*) or MC38 (1×10^6) (*B*) were transplanted s.c into B6 WT mice. After 2 wk, flow cytometric analysis was performed using freshly isolated whole tumor cell preparations in combination with staining of surface markers. CD45.2$^+$ cells were gated, and the expression of indicated surface markers was further analyzed. Numbers represent percentage of the gated and positive cells. A representative experiment of two with similar outcomes is shown. FSC, forward scatter; SSC, side scatter.

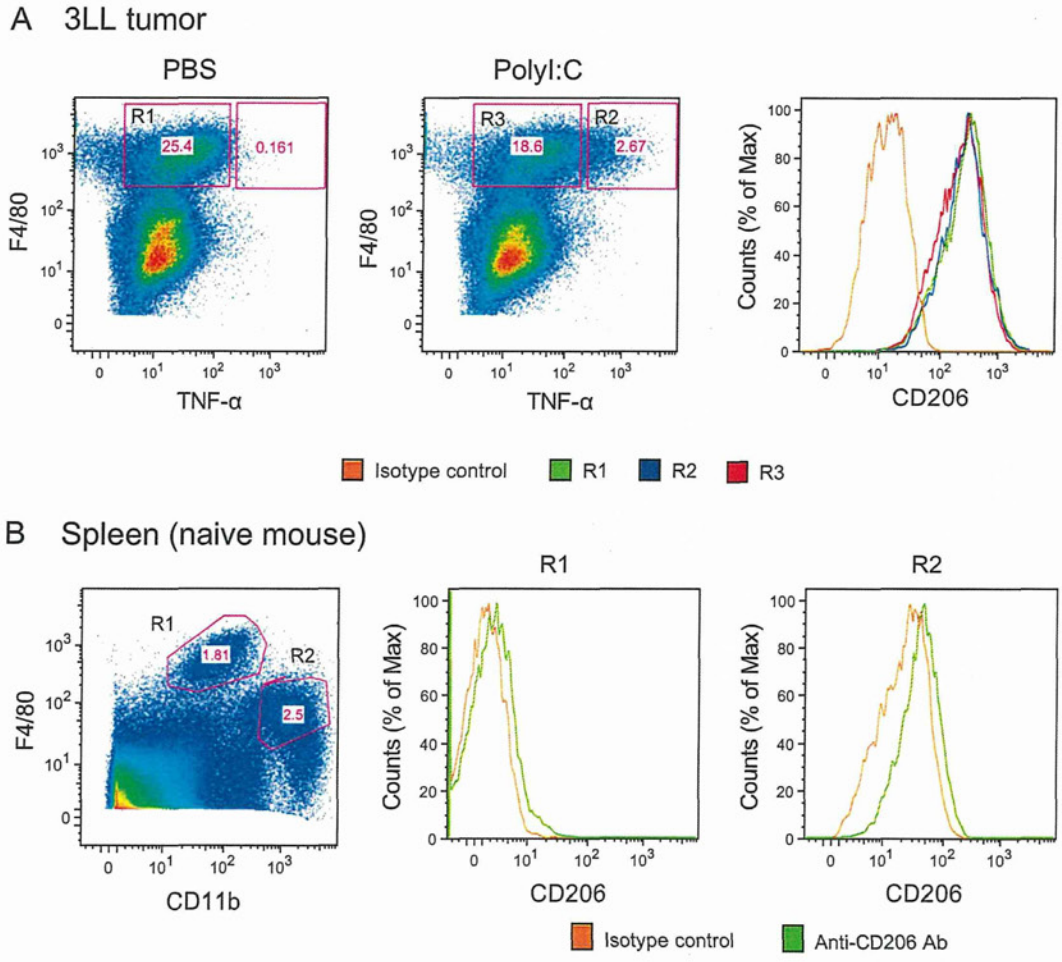

Fig. S6. Both TNF-α–producing and –nonproducing F4/80$^+$ macrophages in 3LL tumor of polyI:C-injected mouse express CD206 (macrophage mannose receptor). (*A*) 3LL tumor-bearing mice were injected i.p with 200 μg polyI:C. After 1 h, single-cell suspension of tumor was incubated in the presence of 10 μg/mL Brefeldin A for 3 h. Intracellular cytokine staining for TNF-α in CD45.2$^+$F4/80$^+$ cells was performed. R2, and R1 and R3 indicates TNF-α–producing and –nonproducing F4/80$^+$ cells, respectively. (*B*) CD206 expression in splenic F4/80$^+$CD11b$^+$ cells (R1 and R2) of naive mouse.

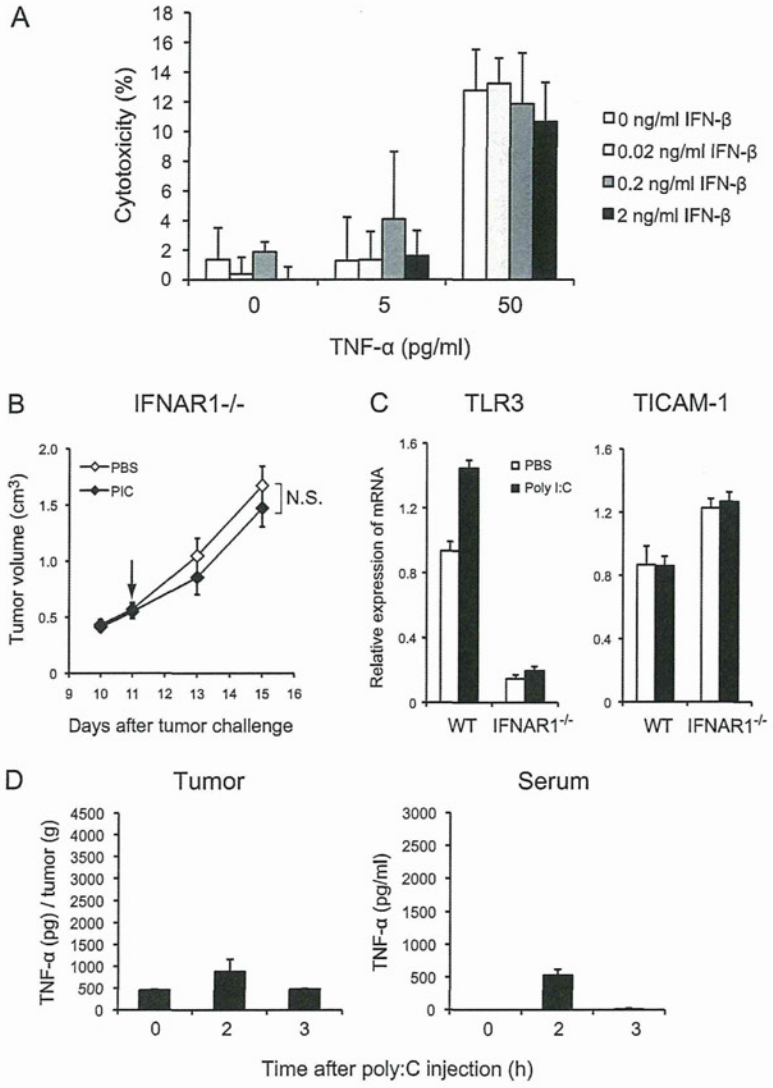

Fig. S7. Involvement of type I IFN signaling in 3LL tumor regression induced by polyI:C. (*A*) Effect of IFN-β on cytotoxic activity of TNF-α against 3LL tumor cells. 3LL cells were incubated in the presence of 0, 5, and 50 pg/mL recombinant mouse TNF-α in combination with 0, 0.02, 0.2, and 2 ng/mL recombinant mouse IFN-β. Cytotoxicity was determined by ^{51}Cr release assay. (*B*) Disabling polyI:C for 3LL tumor regression in IFN-α/β receptor $(IFNAR1)^{-/-}$ mice. PolyI:C was i.p injected on day 11; $n = 3–4$ mice per group. Data are shown as average ± SE. N.S., not significant. (*C*) Levels of the mRNA of TLR3 and TICAM-1 in 3LL tumor-associated $F4/80^{+}$ cells of WT or $IFNAR1^{-/-}$ mice. (*D*) TNF-α levels in tumor and serum in polyI:C-stimulated $IFNAR^{-/-}$ mice. Mice bearing 3LL tumors were i.p. injected with 200 μg polyI:C. Tumor (*Left*) and serum (*Right*) were collected at 0, 2, and 3 h after polyI:C injection, and TNF-α concentration was determined by ELISA. TNF-α level in tumor is presented as [TNF-α protein (pg)/tumor weight (g)].

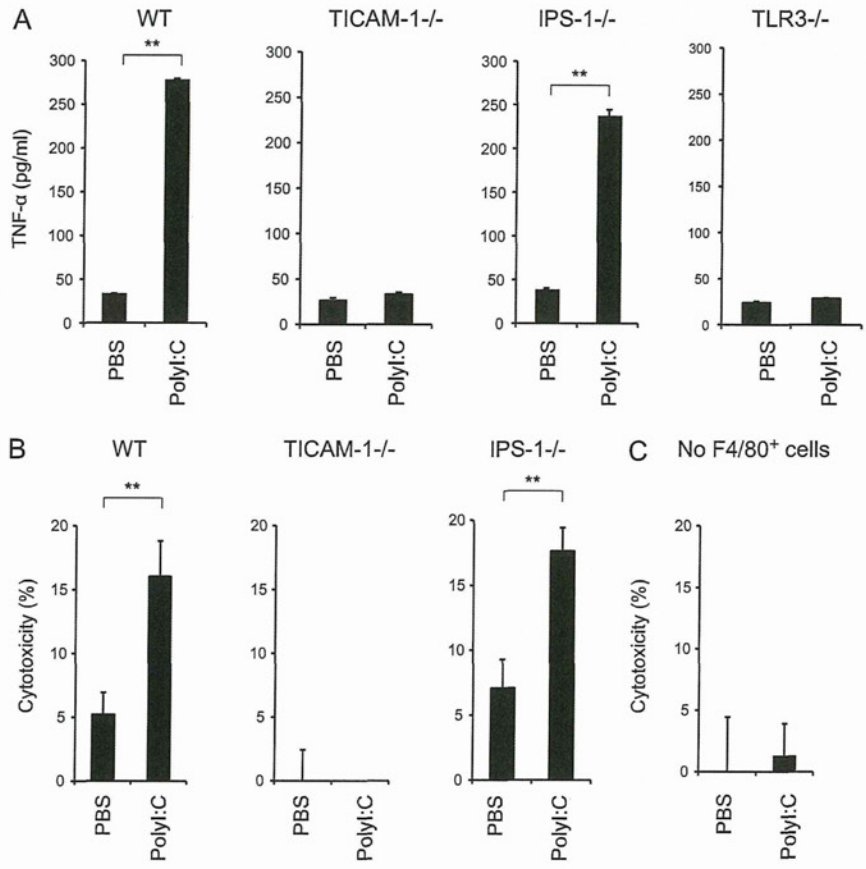

Fig. S8. In vitro polyI:C-stimulated F4/80$^+$ cells secrete TNF-α and have cytotoxic activity. (*A*) F4/80$^+$ cells isolated from 3LL tumor were stimulated with polyI:C (50 μg/mL) in vitro. After 24 h, the conditioned medium was collected and TNF-α concentration was determined by ELISA. (*B*) F4/80$^+$ cells isolated from tumor were mixed with ^{51}Cr-labeled 3LL tumor cells in the presence or absence of polyI:C (50 μg/mL). After 20 h, radioactivity of the conditioned medium was measured. E/T = 10. (*C*) ^{51}Cr-labeled 3LL tumor cells were incubated for 20 h in the presence or absence of polyI:C (50 μg/mL); $n = 3$. Data are shown as average ± SD. $^{**}P < 0.001$. A representative experiment of three with similar outcomes is shown.

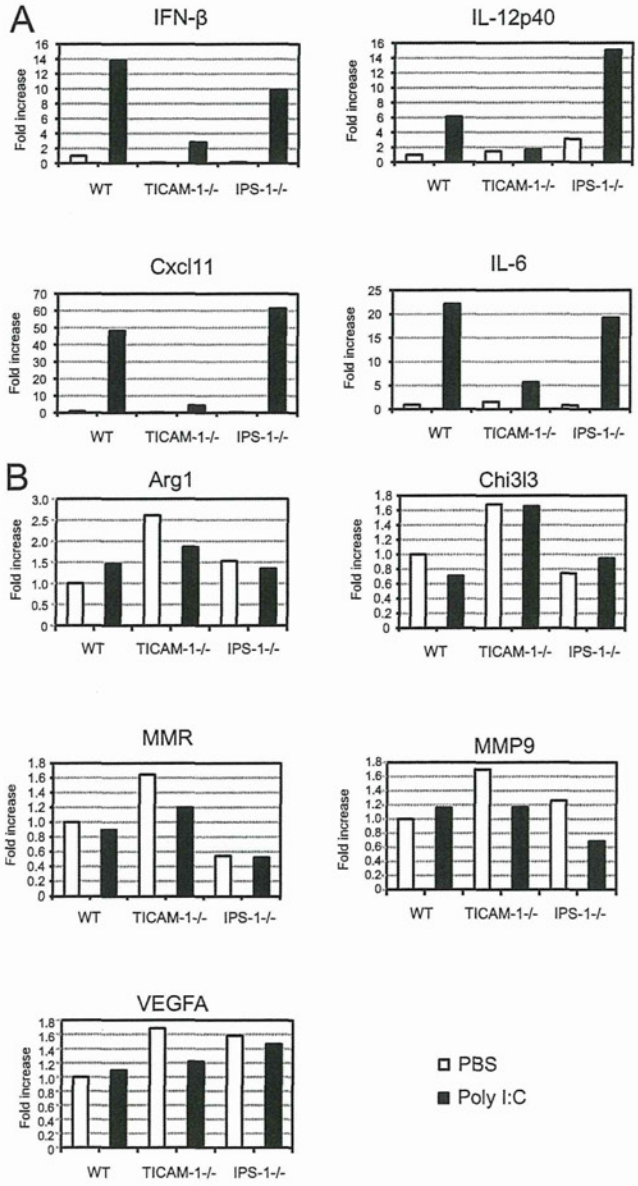

Fig. S9. PolyI:C induces the expression of M1 but not M2 macrophage-associated genes in tumor-infiltrated F4/80$^+$ cells through the TICAM-1 pathway. 3LL tumor-bearing mice were i.p injected with 200 μg polyI:C. After 3 h, tumors pooled from two mice treated with polyI:C or PBS were mixed. F4/80$^+$ cells were isolated from the mixed tumor, and the expression of (*A*) M1- and (*B*) M2-related genes was analyzed. A representative experiment of two with similar outcomes is shown.

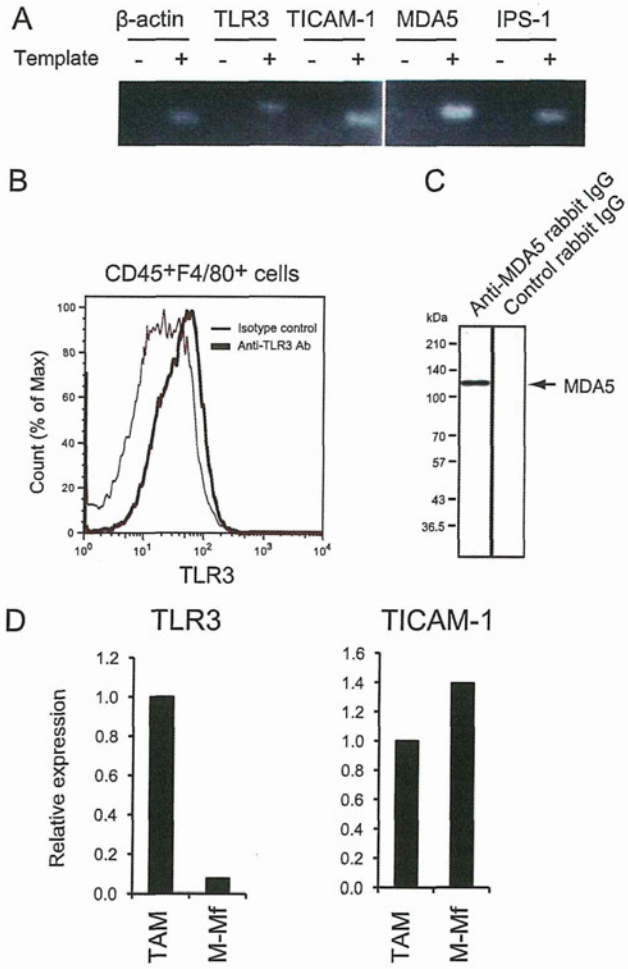

Fig. S10. Expression of TLR3 and MDA5 in 3LL tumor-associated F4/80$^+$ cells. (*A*) mRNA expression of TLR3, TICAM-1, MDA5, and IPS-1 in 3LL tumor-associated F4/80$^+$ cells. Total RNA (1 μg) of F4/80$^+$ cells isolated from 3LL tumor was used as a template for RT-PCR analysis. (*B*) Single-cell suspension of 3LL tumor was stained with FITC-labeled anti-CD45 and PE-labeled anti-F4/80 antibody, followed by intracellular staining with Alexa 647-labeled anti-TLR3 antibody (11F8) or isotype control antibody (rat IgG2a). CD45$^+$F4/80$^+$ cells are shown. (*C*) Cytoplasmic extract of F4/80$^+$ cells was subjected to SDS/PAGE and immunoblotted with rabbit anti-MDA5 antibody or control IgG purified from rabbit serum. (*D*) mRNA expression of TLR3 and TICAM-1 in F4/80$^+$ tumor-associated macrophages (TAM) and macrophage colony-stimulating factor-induced bone marrow-derived macrophages (M-Mf).

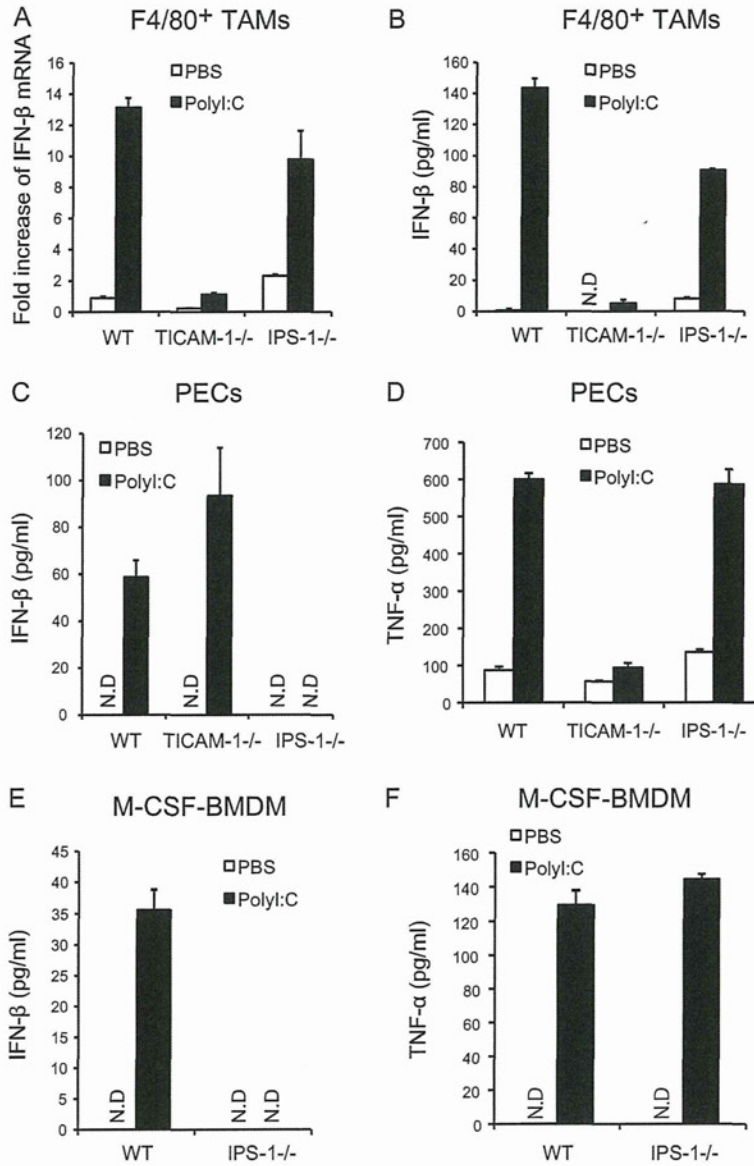

Fig. S11. *In vitro stimulation with polyI:C increases the production of IFN-β and TNF-α by Mfs. (A and B) F4/80+ cells were isolated from 3LL tumor implanted in* WT, TICAM-1$^{-/-}$, and IPS-1$^{-/-}$ mice and stimulated with 50 μg/mL polyI:C. After 4 h, cells were harvested and IFN-β mRNA expression was analyzed by quantitative PCR analysis (*A*). After 20 h, IFN-β concentration in culture supernatant was determined by ELISA (*B*). (*C* and *D*) Peritoneal exudate cells (PECs) isolated from WT, TICAM-1$^{-/-}$, and IPS-1$^{-/-}$ mouse were stimulated with 50 μg/mL polyI:C for 20 h. The concentrations of IFN-β (*C*) and TNF-α (*D*) in culture supernatant were determined by ELISA. (*E* and *F*) Macrophage colony-stimulating factor (M-CSF)-induced bone marrow-derived macrophages (BMDM) were prepared from WT and IPS-1$^{-/-}$ mouse and cultured in the presence of 30% L929 supernatant containing M-CSF. After 6 d, adherent cells were harvested and stimulated with 50 μg/mL polyI:C for 20 h. The concentrations of IFN-β (*E*) and TNF-α (*F*) in culture supernatant were determined by ELISA. Data are shown as mean ± SD ($n = 3$). N.D., not detected. A representative experiment of two with similar outcomes is shown.

Table S1. Expression of various markers on 3LL and MC38 tumor cells

Surface marker	3LL	MC38
H2-K^b	–	++
H2-D^b	±	++
RAE1	++	Not determined
CD45	–	–

Expression of surface markers was analyzed by flow cytometry. Expression was evaluated by mean fluorescence shift: –, ~0.99 ; ±, 1~10 ; +, 11~100 ; ++, 101~.

Table S2. RT-PCR primers used in this study

	Forward primer (5′–3′)	Reverse primer (5′–3′)
IFN-β	CCAGCTCCAAGAAAGGACGA	CGCCCTGTAGGTGAGGTTGAT
IL-12p40	AATGTCTGCGTGCAAGCTCA	ATGCCCACTTGCTGCATGA
IL-6	GTGCATCATCGTTGTTCATACAATC	CTGGGAAATCGTGGAAATGAG
TNF-α	AGGGATGAGAAGTTCCCAAATG	GCTTGTCACTCGAATTTTGAGAAG
IL-1β	TGACGGACCCCAAAAGATGA	TGCTGCTGCGAGATTTGAAG
IL-10	GGCGCTGTCATCGATTTCTC	TGCTCCACTGCCTTGCTCTTA
Cxcl11	GGCTGCGACAAAGTTGAAGTGA	TCCTGGCACAGAGTTCTTATTGGAG
IRF4	AGCCCAGCAGGTTCATAACTACA	CCTCGTGGGCCAAACGT
IRF5	GGTCAACGGGGAAAAGAAACT	CATCCACCCCTTCAGTGTACT
Jmjd3	CGAGTGGTTCGCGGTACAT	GAAGCGGTAAACAGGAATATTGGA
Arg1	GGAATCTGCATGGGCAACCTGTGT	AGGGTCTACGTCTCGCAAGCCA
MMP9	CAAGTGGGACCATCATAACATCA	GATCATGTCTCGCGGCAAGT
VEGFA	GACATCTTCCAGGAGTACC	TGCTGTAGGAAGCTCATCT
Chi3l3	TCACTTACACACATGAGCAAGAC	CGGTTCTGAGGAGTAGAGACCA
Mrc1	CTCTGTTCAGCTATTGGACGC	CGGAATTTCTGGGATTCAGCTTC
Retnla	CCAATCCAGCTAACTATCCCTCC	ACCCAGTAGCAGTCATCCCA
GAPDH	GCCTGGAGAAACCTGCCA	CCCTCAGATGCCTGCTTCA

Table S3. Expression of surface markers on tumor-infiltrated F4/80$^+$ cells

Marker	Expression*
I-Ab	+
H2-D^b	+
H2-K^b	+
CD80	++
CD86	++
CD40	±
CD11c	±
CD3	–
CD4	–
CD8α	–
Gr1	+
B220	+
CD11b	+++
CD206 (MMR)	++

*Expression was evaluated by mean fluorescence shift: –, ~0.99 ; ±, 1 ~10 ; +, 11 ~100 ; ++, 101 ~1,000 ; +++, 1,001~.

Journal of Virology

The Toll-Like Receptor 3-Mediated Antiviral Response Is Important for Protection against Poliovirus Infection in Poliovirus Receptor Transgenic Mice

Yuko Abe, Ken Fujii, Noriyo Nagata, Osamu Takeuchi, Shizuo Akira, Hiroyuki Oshiumi, Misako Matsumoto, Tsukasa Seya and Satoshi Koike

***J. Virol.* 2012, 86(1):185. DOI: 10.1128/JVI.05245-11.**
Published Ahead of Print 9 November 2011.

JVI
Journals.ASM.org

The Toll-Like Receptor 3-Mediated Antiviral Response Is Important for Protection against Poliovirus Infection in Poliovirus Receptor Transgenic Mice

Yuko Abe,[a] Ken Fujii,[a] Noriyo Nagata,[b] Osamu Takeuchi,[c] Shizuo Akira,[c] Hiroyuki Oshiumi,[d] Misako Matsumoto,[d] Tsukasa Seya,[d] and Satoshi Koike[a]

Neurovirology Project, Tokyo Metropolitan Institute of Medical Science, 2-1-6 Kamikitazawa, Setagaya-ku, Tokyo 156-8506, Japan[a]; Department of Pathology, National Institute of Infectious Diseases, 4-7-1 Gakuen, Musashimurayama, Tokyo 208-0011, Japan[b]; Laboratory of Host Defense, WPI Immunology Frontier Research Center (IFReC), Osaka University, 3-1 Yamada-oka, Suita, Osaka 565-0871, Japan[c]; and Department of Microbiology and Immunology, Hokkaido University Graduate School of Medicine, Kita 15, Nishi 7, Kita-ku, Sapporo 060-8638, Japan[d]

RIG-I-like receptors and Toll-like receptors (TLRs) play important roles in the recognition of viral infections. However, how these molecules contribute to the defense against poliovirus (PV) infection remains unclear. We characterized the roles of these sensors in PV infection in transgenic mice expressing the PV receptor. We observed that alpha/beta interferon (IFN-α/β) production in response to PV infection occurred in an MDA5-dependent but RIG-I-independent manner in primary cultured kidney cells *in vitro*. These results suggest that, similar to the RNA of other picornaviruses, PV RNA is recognized by MDA5. However, serum IFN-α levels, the viral load in nonneural tissues, and mortality rates did not differ significantly between MDA5-deficient mice and wild-type mice. In contrast, we observed that serum IFN production was abrogated and that the viral load in nonneural tissues and mortality rates were both markedly higher in TIR domain-containing adaptor-inducing IFN-β (TRIF)-deficient and TLR3-deficient mice than in wild-type mice. The mortality rate of MyD88-deficient mice was slightly higher than that of wild-type mice. These results suggest that multiple pathways are involved in the antiviral response in mice and that the TLR3-TRIF-mediated signaling pathway plays an essential role in the antiviral response against PV infection.

Poliovirus (PV), which belongs to the genus *Enterovirus* in the family *Picornaviridae*, is the causative agent of poliomyelitis (38). The host range of PV is restricted to primates (18). This species' tropism is determined primarily by the cellular PV receptor (PVR; CD155), which gives the virus access to susceptible cells (14–16, 20). Mice are generally not susceptible to PV. However, transgenic mice expressing human PVR (PVR-tg mice) become susceptible to PV and develop a paralytic disease similar to human poliomyelitis after the administration of PV intravenously, intraperitoneally, intracerebrally, or intramuscularly but not orally (26, 40). PV shows a neurotropic phenotype in both humans and PVR-tg mice. PV preferentially replicates in neurons, especially in motor neurons in the anterior or ventral horn of the spinal cord and in the brainstem. However, the efficiency of PV replication is low in nonneural tissues (4, 25). We previously found that innate immune responses that are mediated by type I interferons (IFNs) play important roles in controlling viral replication in nonneural tissues and in the mortality rates of PVR-tg mice (19). In PVR-tg mice deficient in IFNAR1, PV efficiently replicates in nonneural tissues such as the liver, pancreas, and spleen, which are not normal targets of PV. IFNAR1-deficient mice die after the inoculation of a small amount of PV by peripheral routes. The results suggest that the type I IFN response forms an innate immune barrier that prevents PV replication in nonneural tissues and subsequent PV invasion of the central nervous system (CNS). This response therefore plays important roles in the tissue tropism and pathogenicity of PV (25).

The sensors that are involved in the production of type I IFNs in response to RNA viral infections have been recently identified and characterized (1, 46–48). The RIG-I-like receptors (RLRs) retinoic-acid-inducible gene 1 (RIG-I) and melanoma differentiation-associated gene 5 (MDA5) are expressed in the cytoplasm of all cell types, with the exception of plasmacytoid dendritic cells (pDCs). RIG-I and MDA5 have RNA binding domains and differentially recognize specific characteristics of nonself viral RNAs (17, 22, 36, 37). In addition, RLRs have DExD/H box RNA helicase domains (51) that activate downstream signaling pathways resulting in the activation of IFN regulatory factor 3 (IRF-3) and IRF-7 (53). TLR3 and TLR7 are the sensors for viral double-stranded RNA (dsRNA) and single-stranded RNA, respectively (2, 8, 12). TLR3 is expressed in the endosome of macrophages and conventional dendritic cells (DCs) (28) but not in pDCs. TLR3 is also expressed in a variety of epithelial cells, including airway, uterine, corneal, vaginal, cervical, biliary, and intestinal epithelial cells, which may function as efficient barriers to infection. The TLR3-mediated signaling pathway is transmitted through Toll–interleukin-1 (IL-1) receptor (TIR)-containing adaptor molecule 1, which is also known as TIR domain-containing adaptor inducing IFN-β (TRIF), and finally results in the activation of IRF3 and IRF7 (13, 34, 51). TLR7 is specifically expressed in the endosome of pDCs and contributes to the production of a large amount of IFNs in response to many RNA virus infections (5, 7). TLR7 signaling is mediated by the adaptor molecule myeloid differentiation factor 88 (MyD88). These sensors do not contribute equally

Received 29 May 2011 Accepted 20 October 2011
Published ahead of print 9 November 2011
Address correspondence to Satoshi Koike, koike-st@igakuken.or.jp.

doi:10.1128/JVI.05245-11

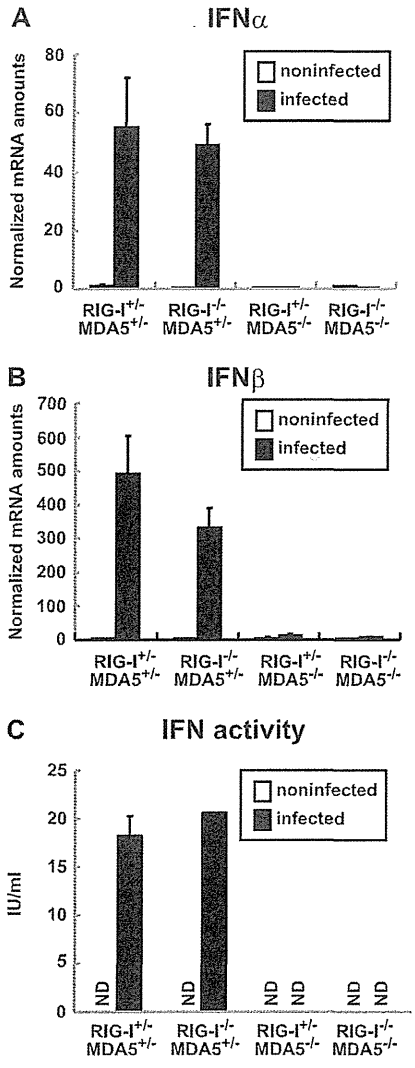

FIG 1 Production of IFNs in primary cultured kidney cells prepared from RIG-I- and MDA5-deficient mice. Kidney cells were pretreated with 100 U of IFN-β for 2 h and infected with PV at an MOI of 10. RNA was prepared from the infected cells at 6 hpi. The amounts of IFN-α mRNA (A) and IFN-β mRNA (B) were determined using quantitative real-time PCR. Cells were prepared in duplicate, and the experiments were repeated three times. Representative data are shown. The amount of IFN activity in the supernatant of infected kidney cells at 8 hpi was determined by the cytopathic effect dye uptake method using L929 cells (C). ND, not detected.

to the antiviral response to each viral infection. The type I IFN production that is induced by these sensors occurs in a virus-specific and cell-specific manner (21, 23). For example, RIG-I plays an important role in the antiviral response to Newcastle disease virus, influenza A virus, Sendai virus, vesicular stomatitis virus, Japanese encephalitis virus, and hepatitis C virus. However, MDA5 is important in the response to infection with picornaviruses, such as encephalomyocarditis virus (EMCV) (10, 23). Although RNA viruses produce dsRNA during the replication step, the protective effect of the TLR3-mediated pathway is not clear (9). In a previous study, TLR3 expression was found to cause severe encephalitis in West Nile virus (WNV) infection (50). How these sensor molecules contribute to the recognition of PV infection is not understood. The aim of the present study was to determine the role of these sensors in the response to PV infection in transgenic mice expressing human PVR. We generated PVR-tg mice deficient in these sensor and adaptor molecules. Our results demonstrate that the MDA5-, TRIF- and MyD88-mediated pathways contribute to the antiviral response against PV infection and that the TLR3-TRIF-mediated pathway plays a pivotal role in this response.

MATERIALS AND METHODS

Cells and viruses. An AGMK cell line, JVK-03 (24), was maintained in Eagle's minimum essential medium containing 5% fetal bovine serum. PV type I Mahoney, a strain derived from the infectious cDNA clone pOM, was used in this study (45). The virus was propagated in JVK-03, and the viral titer was determined using the plaque assay. Primary cultured kidney cells were prepared from transgenic and knockout mice as previously described (54).

Transgenic and knockout mice and infection experiments. All experiments using mice were performed in accordance with the Guidelines for the Care and Use of Laboratory Animals of the Tokyo Metropolitan Institute of Medical Science. ICR-PVRTg21 mice (26) were mated with RIG-I$^{-/-}$ and/or MDA5$^{-/-}$ mice (21) in the ICR background because it is difficult to maintain RIG-I$^{-/-}$ mice in other genetic backgrounds. We mated mice and obtained littermates with the genotypes RIG-I$^{+/-}$ MDA5$^{+/-}$, RIG-I$^{-/-}$ MDA5$^{+/-}$, RIG-I$^{+/-}$ MDA5$^{-/-}$, and RIG-I$^{-/-}$ MDA5$^{-/-}$ to use in experiments. C57BL/6 (B6)-PVRTg21 mice were mated with MDA5$^{-/-}$ mice, TRIF$^{-/-}$ mice, MyD88$^{-/-}$ mice, and TLR3$^{-/-}$ mice (51) in the B6 background (backcrossed 7 to 10 times). IFNAR1$^{-/-}$ PVR-tg mice were previously described (19). Because all of the mice that were used in the present study were in the PVR-tg background, we omitted the notation "PVR-tg" for simplicity in this report. Six- to 7-week-old mice were used for infection experiments. The survival and clinical symptoms of the mice were observed daily for 3 weeks. At the first sign of severe neurological symptoms, the mice were sacrificed as a humane endpoint.

Measurement of IFN levels. IFN-α levels in the sera were determined using an enzyme-linked immunosorbent assay (ELISA). The ELISA kit for IFN-α was purchased from PBL Biochemical Laboratories. Mouse IFN activity in the supernatants of PV-infected kidney cells was measured by the cytopathic effect dye uptake method using L929 cells (54, 55). Recombinant mouse IFN-β (Toray) was used as the standard for unit definition.

Quantitative real-time reverse transcription (RT)-PCR. RNA was isolated from the tissues of infected mice or infected cells using the Isogen RNA extraction kit (Nippon Gene). DNase I treatment and cDNA synthesis were performed as previously described (54). The amounts of the mRNAs for IFN-α, IFN-β, OAS1a, and IRF-7 were determined using real-time RT-PCR with an ABI Prism 7500 (Applied Biosystems) as previously described (54).

RESULTS

IFN production in primary cultured kidney cells is dependent on MDA5. We examined whether, similar to EMCV infection, PV infection is recognized by MDA5 *in vitro*. We mated PVR-tg mice with MDA5-deficient and RIG-I-deficient mice to generate RIG-I$^{+/-}$ MDA5$^{+/-}$, RIG-I$^{-/-}$ MDA5$^{+/-}$, RIG-I$^{+/-}$ MDA5$^{-/-}$, and RIG-I$^{-/-}$ MDA5$^{-/-}$ mice in the ICR background. We prepared primary cultured kidney cells from mice with these genotypes to determine the role of RLRs. After cultivation for approximately 1 week, the cells that became confluent were infected with PV at a multiplicity of infection (MOI) of 10. RNA was recovered from the infected cells at 6 hpi, and the amounts of the mRNAs for IFN-α and IFN-β were determined using real-time RT-PCR. Kid-

ney cells that were not pretreated with IFN-β before PV infection showed rapid cytopathic effect progression and did not produce IFN mRNA (data not shown). This result is consistent with our previous observations (54). We therefore pretreated cells with 100 U of IFN-β for 2 h and infected them with PV. As we reported previously, the IFN-treated kidney cells became resistant to PV infection, PV replication was severely inhibited, and IFN production was observed (54). Under this condition, we determined the sensor responsible for IFN production. We observed the induction of both IFN-α (Fig. 1A) and IFN-β mRNAs (Fig. 1B) in cells that were isolated from RIGI-I$^{+/-}$ MDA5$^{+/-}$ mice and RIGI-I$^{-/-}$ MDA5$^{+/-}$ mice but not from RIGI-I$^{+/-}$ MDA5$^{-/-}$ mice or RIGI-I$^{-/-}$ MDA5$^{-/-}$ mice. The induced IFN proteins were not detected by ELISA due to a very small amount of IFNs produced in the supernatants. However, IFN activity was detected in the supernatants of PV-infected kidney cells prepared from RIGI-I$^{+/-}$ MDA5$^{+/-}$ mice and RIGI-I$^{-/-}$ MDA5$^{+/-}$ mice but not from RIGI-I$^{+/-}$ MDA5$^{-/-}$ mice or RIGI-I$^{-/-}$ MDA5$^{-/-}$ mice using the cytopathic effect dye uptake method (Fig. 1C). These results suggest that PV infection is recognized by MDA5 but not RIG-I in primary murine kidney cells, which is consistent with previous reports demonstrating that MDA5 is essential for the detection of picornaviruses (10, 23). However, MDA5-mediated IFN production was observed only when cells had been primed with a low dose of IFNs.

IFN responses of MDA5-deficient mice are not significantly different from those of wild-type mice. We hypothesized that MDA5 plays an important role in the type I IFN response upon PV infection *in vivo*. We examined the serum IFN-α levels in PVR-tg mice intravenously infected with 2×10^7 PFU of PV using ELISA. Their serum IFN-α level was initially observed at 9 hpi, peaked at 12 hpi, and began to decline at 24 hpi (Fig. 2A). We then determined the serum IFN-α levels of the knockout mice at 12 hpi. Unexpectedly, similar serum IFN-α levels were detected in RIG-I$^{+/-}$ MDA5$^{+/-}$, RIG-I$^{+/-}$ MDA5$^{-/-}$, RIG-I$^{-/-}$ MDA5$^{+/-}$, and RIG$^{-/-}$ MDA5$^{-/-}$ mice infected with PV (Fig. 2B).

We monitored the induction of mRNAs for the IFN-stimulated genes (ISGs), OAS1a (Fig. 3A) and IRF-7 (Fig. 3B), in the brain, spinal cord, liver, spleen, and kidney using real-time RT-PCR. Among the organs tested, the expression levels of these ISGs were the highest in the spleen. However, the expression profiles of these genes were essentially the same in all organs. In accordance with the elevated serum IFN levels, the induction of ISGs in various organs was observed in all mice (Fig. 3A and B). The results suggest that MDA5 does not play a critical role in IFN production and subsequent ISG induction in response to PV infection *in vivo*.

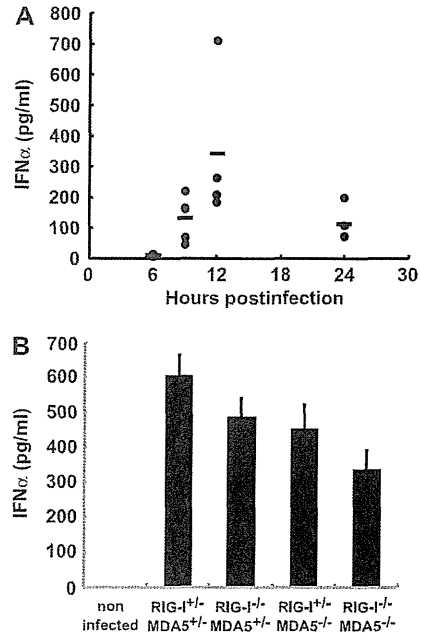

FIG 2 Production of serum IFN-α in RIG-I- and MDA5-deficient mice. (A) Time course of IFN-α levels in serum. PVR-tg mice in the B6 background (n = 4 or n = 5) were intravenously infected with 2×10^7 PFU of PV. Serum samples were collected at the indicated time points, and the concentration of IFN-α was determined using ELISA. (B) IFN-α levels of RIG-I- and MDA5-deficient mice in the ICR background (n = 8) at 12 hpi were compared. The experiments were repeated twice, and representative data are shown.

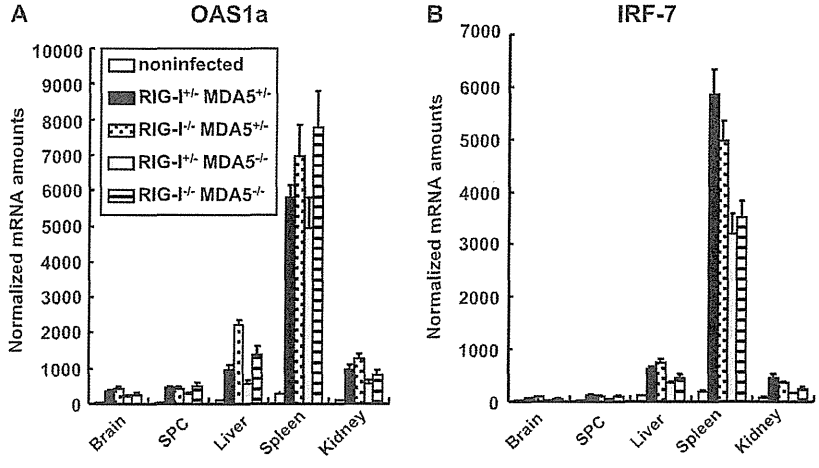

FIG 3 ISG induction in RIG-I- and MDA5-deficient mice. Mice (n = 4) were intravenously infected with 2×10^7 PFU of PV. At 12 hpi, RNA was isolated from the indicated tissues of the infected mice and OAS1a (A) and IRF-7 (B) mRNA levels were determined using quantitative real-time PCR. The experiments were repeated twice, and representative data are shown. SPC, spinal cord.

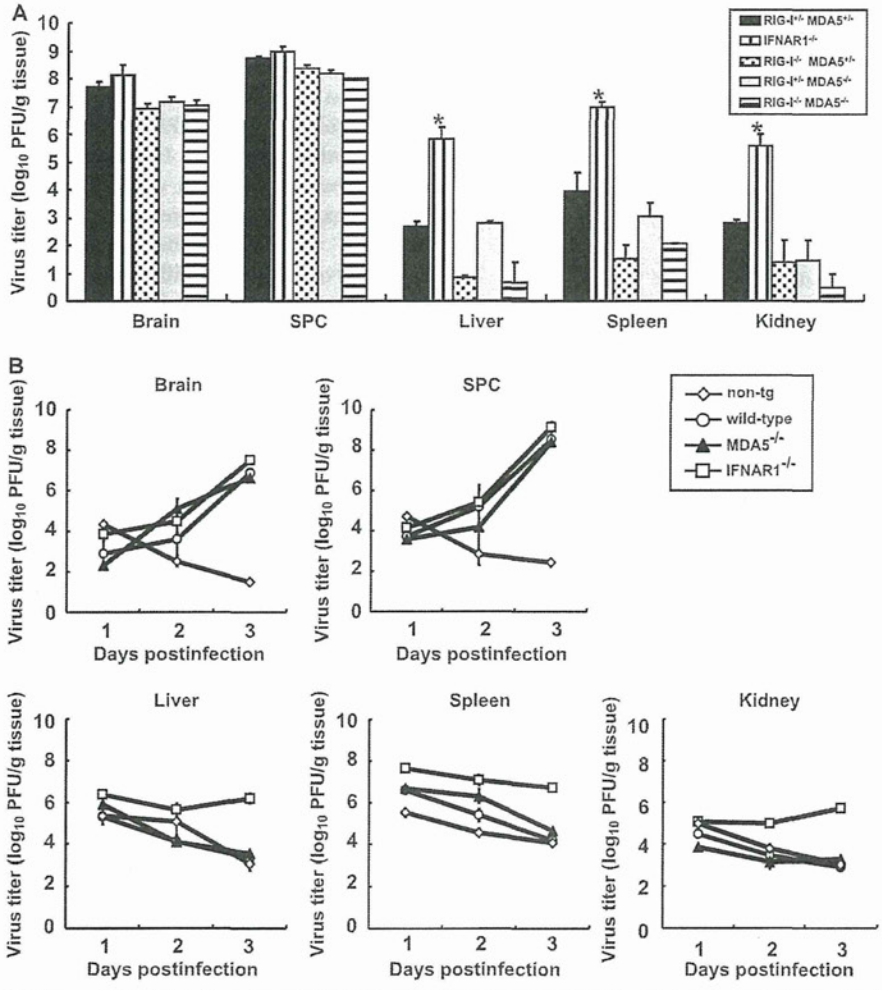

FIG 4 (A) PV replication in RIG-I- and MDA5-deficient mice. RIGI-I$^{+/-}$ MDA5$^{-/-}$, RIGI-I$^{-/-}$ MDA5$^{+/-}$, RIGI-I$^{-/-}$ MDA5$^{+/-}$, and RIGI-I$^{-/-}$ MDA5$^{-/-}$ mice in the ICR background and IFNAR1$^{-/-}$ mice in the B6 background ($n = 3$) were intravenously infected with 2×10^7 PFU of PV. Infected mice were paralyzed or dead at 3 to 5 days postinfection. The tissues of the paralyzed mice were collected, and the viral titers were determined using a plaque assay (*, $P < 0.01$ by t test compared to RIGI-I$^{+/-}$ MDA5$^{+/-}$ mice). (B) PV replication kinetics in MDA5-deficient mice. Nontransgenic (non-tg) mice, wild-type mice, MDA5$^{-/-}$ mice, and IFNAR1$^{-/-}$ mice in the B6 background ($n = 3$) were infected as described above. Tissues were collected daily, and viral titers were determined. SPC, spinal cord.

PV replication in nonneural tissues and mortality rates of mice deficient in RIG-I-like receptors. We have previously shown that the IFN-α/β response forms an innate immune barrier to prevent PV replication in nonneural tissues and PV invasion of the CNS (19, 25). Therefore, we evaluated PV replication in neural and nonneural tissues in RLR-deficient mice. The mice were infected with 2×10^7 PFU of PV, which is approximately 100 times higher than the 50% lethal doses for all mouse strains. The infected mice showed paralysis by 3 to 5 days postinfection. The brain, spinal cord, liver, spleen, and kidney of the paralyzed mice were recovered, and their viral titers were determined (Fig. 4A). PV was recovered from the CNS of the paralyzed mice almost equally among the genotypes. The viral titers recovered from the liver, spleen, and kidney of IFNAR1$^{-/-}$ mice were significantly higher than those of wild-type mice, as previously described (19). However, PV titers that were recovered from these organs of RIG-I$^{-/-}$ MDA5$^{+/-}$, RIG-I$^{+/-}$ MDA5$^{-/-}$, and RIG-I$^{-/-}$ MDA5$^{-/-}$ mice were as low as or lower than those in the organs of RIG-I$^{+/-}$ MDA5$^{+/-}$ mice. We then examined virus replication kinetics using nontransgenic mice, wild-type mice, IFNAR$^{-/-}$ mice, and MDA5$^{-/-}$ mice in the B6 background (Fig. 4B). The viral load in the CNS increased in a similar fashion among the transgenic mouse strains. However, the viral load kinetics in the liver, spleen, and kidney of wild-type and MDA5$^{-/-}$ mice were similar to those of nontransgenic mice. The values for nontransgenic mice indicate the kinetics of clearance of inoculated virus. The results indicated that PV replication was severely inhibited in the liver, spleen, and kidney of wild-type and MDA5$^{-/-}$ mice. This inhibition correlated well with the induction of serum IFNs in MDA5$^{-/-}$ mice (Fig. 2). The PV antigen was detected in neurons in the CNS but not in other tissues in all knockout mice (Table 1). This result indicates that the lack of RLRs did not alter the tissue tropism of PV. These data suggest that inhibition of PV replication in nonneural tissues is not dependent on RLRs and that MDA5-independent mechanisms are the major contributors in controlling PV replication.

We examined the mortality rates of RIG-I$^{+/-}$ MDA5$^{+/-}$, RIG-I$^{-/-}$ MDA5$^{+/-}$, RIG-I$^{+/-}$ MDA5$^{-/-}$, and RIG-I$^{-/-}$ MDA5$^{-/-}$